The Astrophysical Journal, 685:622–628, 2008 September 20

STRONGLY BLUESHIFTED PHENOMENA OBSERVED WITH *HINODE* EIS IN THE 2006 DECEMBER 13 SOLAR FLARE

Ayumi Asai,[1,2,3] Hirohisa Hara,[2,3] Tetsuya Watanabe,[2,3] Shinsuke Imada,[2] Taro Sakao,[4] Noriyuki Narukage,[4] J. L. Culhane,[5] and G. A. Doschek[6]
Received 2008 January 5; accepted 2008 May 28

ABSTRACT

We present a detailed examination of strongly blueshifted emission lines observed with the EUV Imaging Spectrometer on board the *Hinode* satellite. We found two kinds of blueshifted phenomenon associated with the X3.4 flare that occurred on 2006 December 13. One was related to a plasmoid ejection seen in soft X-rays. It was very bright in all the lines used for the observations. The other was associated with the faint arc-shaped ejection seen in soft X-rays. The soft X-ray ejection is thought to be a magnetohydrodynamic (MHD) fast-mode shock wave. This is therefore the first spectroscopic observation of an MHD fast-mode shock wave associated with a flare.

Subject headings: Sun: corona — Sun: flares — Sun: transition region — Sun: UV radiation — Sun: X-rays, gamma rays

1. INTRODUCTION

Solar flares are very spectacular, and they are accompanied by a variety of plasma motions. For example, many ejection phenomena, such as filament/prominence eruptions, are seen in the Hα line and in the extreme-ultraviolet (EUV), while plasmoid ejections seen in soft X-ray (SXR) have been observed in association with solar flares. They have attracted attention, since they could play a key role in triggering fast reconnection. In the plasmoid-induced reconnection model, which was suggested by Shibata (1999) and Shibata & Tanuma (2001) as an extension of the classical CSHKP model (Carmichael 1964; Sturrock 1966; Hirayama 1974; Kopp & Pneuman 1976), plasmoids generated in current sheets near reconnection points are ejected when strong energy releases occur. The ejections of plasmoids trigger further reconnections, since they make the current sheet thinner. We often observe that plasmoids/filaments are strongly accelerated during bursts of nonthermal emissions in hard X-ray (HXR) and in radio (Kahler et al. 1988; Shibata et al. 1995; Tsuneta 1997; Ohyama & Shibata 1998; Morimoto & Kurokawa 2003; Sterling & Moore 2004, 2005). Therefore, the correlations between plasmoid ejections and HXR bursts support a plasmoid-induced reconnection model. A good review of the correlation between plasmoid ejections and HXR emission is given in Aschwanden (2002).

Flare-associated waves and the related plasma motions have also been studied. Moreton waves (Moreton 1960; Smith & Harvey 1971) are observed to propagate across the solar disk in Hα with speeds of 500–1500 km s^{-1} (e.g., Eto et al. 2002; Warmuth et al. 2004a, 2004b). They are often associated with type II radio bursts and thought to be due to the intersection of a coronal MHD fast-mode shock wave and the chromosphere (Uchida 1968, 1970; Uchida et al. 1973). X-ray waves discovered with the Soft X-Ray Telescope (SXT; Tsuneta et al. 1991) on board *Yohkoh* (Ogawara et al. 1991) are the wavelike disturbances traveling in the solar corona associated with flares (Khan & Hudson 2000; Khan & Aurass 2002; Hudson et al. 2003). The simultaneous observation of Moreton waves and X-ray waves suggest that both of these wavelike disturbances are generated with the MHD fast-mode shock (Khan & Aurass 2002; Narukage et al. 2002). Furthermore, the Solar X-Ray Imager on board *GOES* has also observed wavelike disturbances in X-rays (Warmuth et al. 2005). Coronal waves observed with the Extreme-Ultraviolet Imaging Telescope (EIT; Delaboudiniére et al. 1995) on board the *Solar and Heliospheric Observatory* (*SOHO*; Domingo et al. 1995) are another coronal disturbance (e.g., Thompson et al. 2000) and are called EIT waves. However, these coronal disturbances have rarely been observed spectroscopically in EUV and in SXR. Therefore, spectroscopic observations of wavelike ejections with high spatial and spectral resolution are required to clarify the relation with the MHD fast-mode shock.

These plasma motions can be observed as phenomena accompanied by line shifts (Doppler shifts) in spectroscopic observations. The EUV Imaging Spectrometer (EIS; Culhane et al. 2007) is one of the three scientific instruments on board *Hinode* (Kosugi et al. 2007). EIS uses an off-axis parabolic primary mirror and a toroidal diffraction grating in a normal incidence optical layout and has sensitivity for two wavelength ranges, 170–210 and 250–290 Å (see Korendyke et al. [2006] and Lang et al. [2006] for more details). These wavelength ranges are simultaneously observed with two CCDs, which are called CCD-A (for longer wavelength range) and CCD-B (for shorter wavelength range), respectively. The two-dimensional EUV images were obtained with the narrow slit in a raster observation by a pivot rotation of the primary mirror in the east-west direction. EIS enables us to study in detail the plasma in the solar corona and upper transition region with temperature of 8×10^4 to 2×10^7 K.

We found strongly blueshifted phenomena, which were associated with an intense flare that occurred 2006 December 13 observed with EIS. In this paper we examine the phenomena and discuss the relation with plasmoid ejections and/or coronal waves. In § 2 we describe the observational data. In § 3 we examine the

[1] Nobeyama Solar Radio Observatory, National Astronomical Observatory of Japan, Minamimaki, Nagano 384-1305, Japan.
[2] National Astronomical Observatory of Japan, Osawa, Mitaka, Tokyo 181-8588, Japan.
[3] Graduate University for Advanced Studies (SOKENDAI), Hayama, Miura, Kanagawa 240-0193, Japan.
[4] Institute of Space and Astronautical Science, Japan Aerospace Exploration Agency, Yoshinodai, Sagamihara, Kanagawa 229-8510, Japan.
[5] Mullard Space Science Laboratory, University College London, Holmbury St. Mary, Dorking, Surrey RH5 6NT, UK
[6] Naval Research Laboratory, E. O. Hulburt Center for Space Research, Washington, DC 20375-5320.

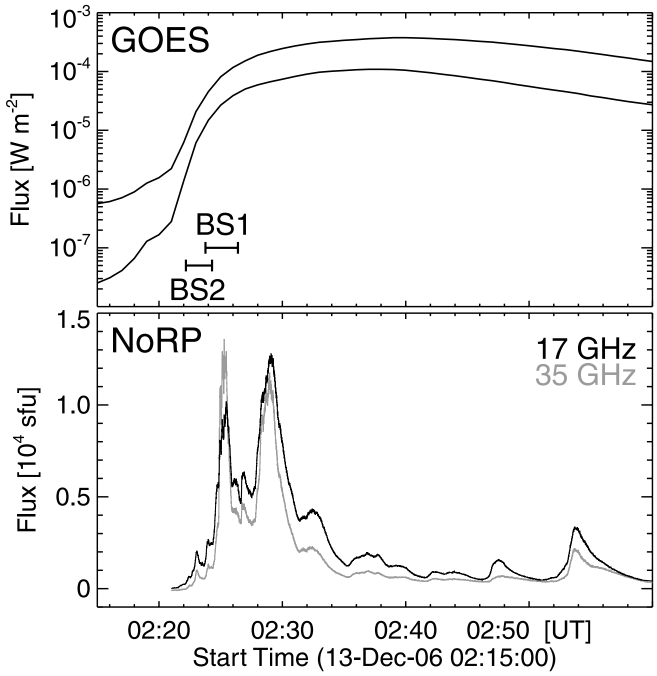

Fig. 1.—Overview of the 2006 December 13 flare. Temporal variations of the *GOES* SXR flux in the 1.0–8.0 and 0.5–4.0 Å channels (*top*) and radio time profiles (17 and 35 GHz) obtained with NoRP (*bottom*). The time ranges of BS1 and BS2 seen in the EIS field of view are marked with BS1 and BS2, respectively.

detailed features of the strongly blueshifted line emission. In § 4 we present a summary and conclusions.

2. OBSERVATIONS

An intense solar flare, which was X3.4 on the *GOES* scale, started at 02:14 UT, 2006 December 13, in NOAA AR 10930 (S06°, W22°). It was the first X-class flare that *Hinode* observed (see also Kubo et al. 2007; Su et al. 2007; Imada et al. 2007; Isobe et al. 2007). Figure 1 (*top*) shows time profiles of the flare (from 02:10 UT to 03:00 UT, 2006 December 13), in SXR obtained with the *GOES* 1.0–8.0 (*top plot*) and 0.5–4.0 Å (*bottom plot*) channels. The Nobeyama Radio Polarimeters (NoRP; Torii et al. 1979; Shibasaki et al. 1979; Nakajima et al. 1985) also observed this flare. Figure 1 (*bottom*) shows the time profiles of the total radio fluxes taken in NoRP 17 GHz (*black line*) and 35 GHz (*gray line*) channels.

EIS performed a wide raster scan from 01:12 to 05:41 UT, and the following nine lines were chosen to observe the flare: Fe x (184.5 Å), Fe viii (185.2 Å), Fe xi (188.2 Å), Ca xvii (192.8 Å), Fe xii (195.1 Å), Fe xiii (202.0 Å), He ii (256.3 Å), Fe xiv (274.2 Å), and Fe xv (284.2 Å). Information on these lines is summarized in Table 1. We used a narrow slit of 1″ width. For each emission line, we set the observation window on the CCDs with a height of 256 pixels along the slit and a width of 24 pixels in the wavelength direction. These correspond to 256″ and 0.54 Å, respectively. We show the raster images in the He ii and Fe xv lines in Figure 2 (*bottom panels*). The field of view (FOV) of CCD-A is displaced southward in the slit direction by about 18″, compared with that of CCD-B. In this work we have corrected for this displacement. The absolute positions of the FOVs are determined with the EUV images observed with other instruments as is described below.

We are focusing on the strongly blueshifted feature observed with EIS. In the impulsive phase two kinds of features are observed. One is located about 120″ south of the disk center, which is just south of the flare core region. This is bright in all lines, and drifts southward with a velocity of about 50 km s^{-1}. The small box drawn with black dotted lines in the bottom right panel of Figure 2 shows the position of this feature. The other blueshifted feature appears farther from the flare core site and is located 200″ south of the disk center. This very faint feature is seen only in high-temperature lines and moves southward with high velocity. We call these features BS1 and BS2, and they are discussed in more detail in § 3.

TABLE 1
Line List Used for the Raster Observation

Target Ion	Center Wavelength (Å)	CCD	log *T*
Fe x	184.5	CCD-B	6.0
Fe viii	185.2	CCD-B	5.6
Fe xi	188.2	CCD-B	6.1
Ca xvii	192.8	CCD-B	6.8
Fe xii	195.1	CCD-B	6.2
Fe xiii	202.0	CCD-B	6.2
He ii	256.3	CCD-A	4.9
Fe xiv	274.2	CCD-A	6.2
Fe xv	284.2	CCD-A	6.4

The imaging observation of this flare in EUV was performed with the *Transition Region and Coronal Explorer* (*TRACE*; Handy et al. 1999; Schrijver et al. 1999), although the impulsive phase was unfortunately missed. We show the 195 Å images of the flare taken by *TRACE* at 02:05:25 UT (*left*) and 02:47:20 UT (*right*) in Figure 2 (*top panels*). We can see a dark filament lying horizontally (i.e., in the east-west direction) in the western part of the active region. It can also be seen in the EIS raster images until 02:20 UT. The dark filament disappeared after the flare started. *SOHO* EIT also observed the eruption of the filament in the 195 Å images, traveling in the southwest direction. We co-aligned the EUV images obtained with EIS, *TRACE*, and EIT by using the 195 Å data. In particular, the EIS raster image was fitted with the *TRACE* preflare (02:05:25 UT) image, by using the common features seen from 02:00 to 02:10 UT. The accuracy of the co-alignment between the EIS and *TRACE* data for the time range is about 1″, which is comparable to the pixel sizes of the data.

The Solar Optical Telescope (SOT; Tsuneta et al. 2007) and X-Ray Telescope (XRT; Golub et al. 2007) on board *Hinode* also observed this flare. The Ca ii (H-line) images obtained every 2 minutes with SOT clearly show the two-ribbon structure (see Fig. 4, *top panels*). XRT obtained the SXR images of this flare every 1 minute with the thin-Be filter. In the SXR images we can see some ejections of bright plasmoids (see Fig. 4, *bottom panels*). We can also see a faint arc-shaped ejection (see Fig. 5, *bottom panels*). We discuss these in § 3. We co-aligned the SOT and XRT data with the *TRACE* data. For the co-alignment, we used common features, such as flare kernels. The accuracy of the co-alignment is also about 1″ and, therefore, we expect that the EIS data are co-aligned with the SOT and XRT data with an accuracy of about 2″.

3. BLUESHIFTED FEATURES

3.1. *The Northern Feature—BS1*

This strong blueshifted feature associated with BS1 appeared from 02:23:46 UT to 02:26:24 UT in the EIS FOV, which corresponds to the first impulsive radio burst observed with NoRP (see Fig. 1). Figure 3 (*top panels*) shows the clipped spectra of BS1 in the He ii (*left*) and Fe xv (*right*) lines. The vertical axis is

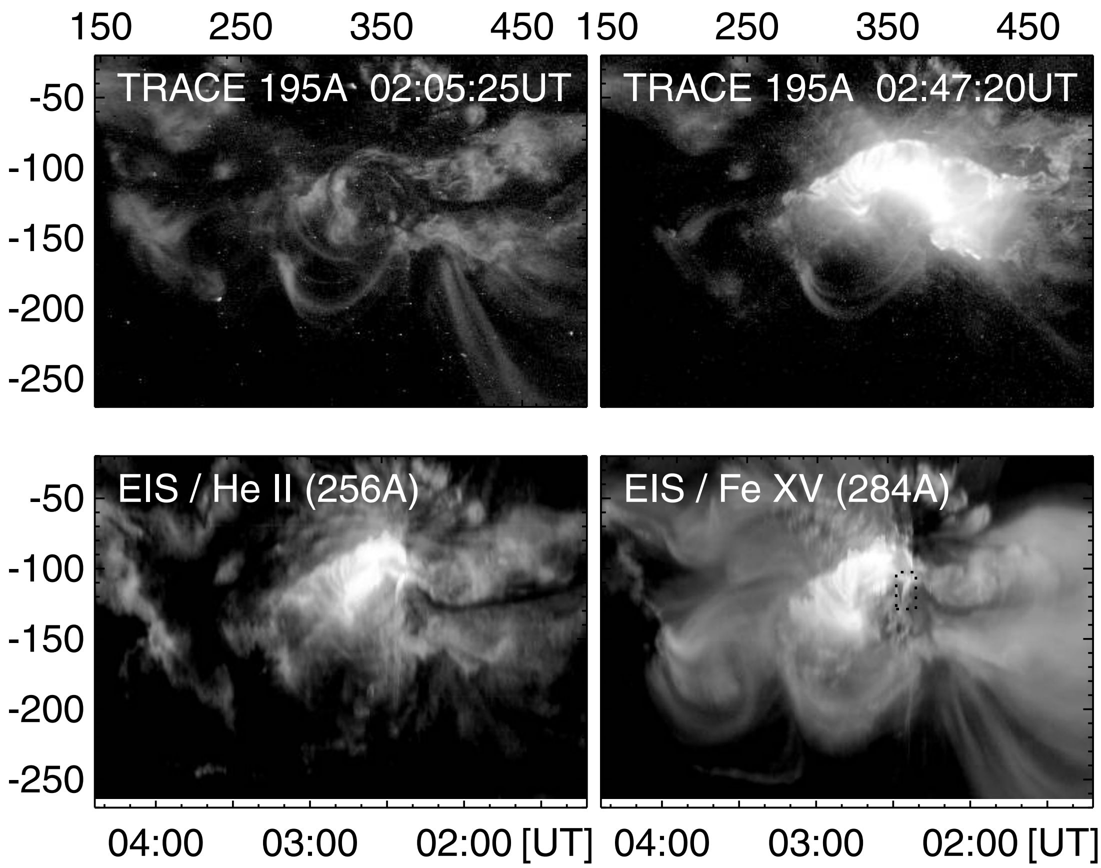

Fig. 2.—EUV (195 Å) images taken with *TRACE* (*top*), and raster images of He II (256 Å: *bottom left*) and in Fe XV (284 Å: *bottom right*) lines. Solar north is up, and west is to the right. The horizontal and vertical axes give the distance from the disk center in arcseconds, as shown in the top panels. For the EIS raster images, the horizontal axis below the panels shows the times. The small box with the dotted line in the bottom right panel points to the BS1 region.

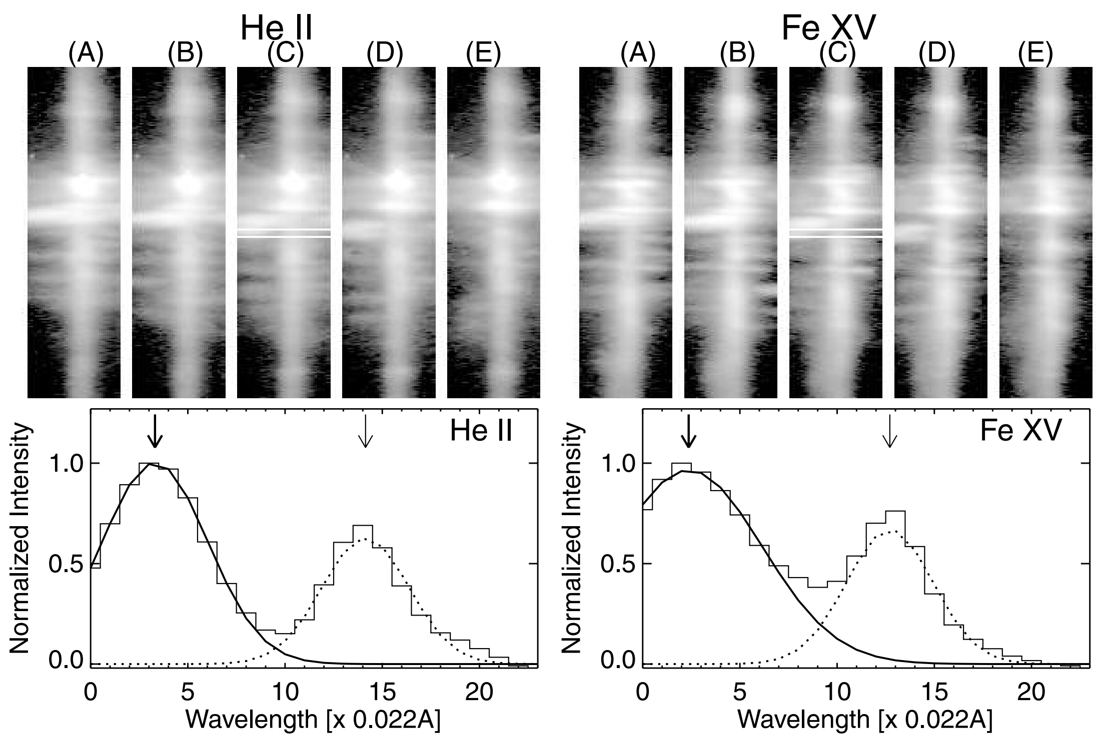

Fig. 3.—Northern blueshift (BS1). *Top*: Time-sequenced spectra of He II (*left*) and Fe XV (*right*) windows observed with *Hinode* EIS. The time of each panel is (A) 02:24:49 UT, (B) 02:25:21 UT, (C) 02:25:52 UT, (D) 02:26:24 UT, and (E) 02:26:56 UT. Solar north is up, and blue is to the left. The size of each window is 224″ along the EIS slit (vertical) and 24 pixels in the CCDs of EIS, which corresponds to 0.54 Å in the wavelength scale (horizontal). *Bottom*: Normalized spectra at BS1 in He II (*left*) and Fe XV (*right*) windows. The solid histograms show the spectra averaged over the region sandwiched between the two horizontal white lines in the top panels. The dotted and solid lines are the fitting results that represent the main and the blueshift components of the line. The peaks of each line are shown with thin and thick arrows.

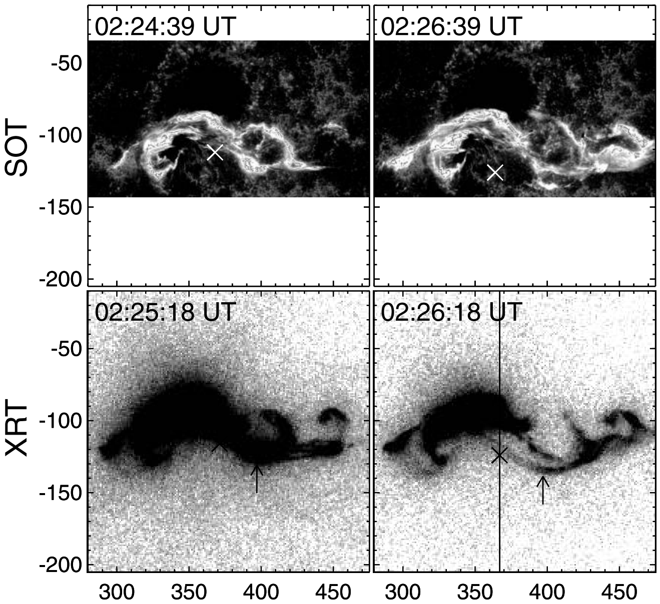

FIG. 4.—*Top*: Ca II (H-line) images taken with *Hinode* SOT. *Bottom*: Soft X-ray images obtained with the *Hinode* XRT (negative images). Solar north is up, and west is to the right. The horizontal and vertical axes give the distance from the disk center in arcseconds, as shown in the top and the left. The crosses ($\times$) point to the positions of BS1. The arrows in the bottom right panel follow the plasmoid ejection seen in XRT. The vertical line in the bottom right panel shows the position of the EIS slit. The slit extends from $y = -233''$ to $-9''$.

the extent along the slit (the solar north is up), and the size is 224″ ($\sim 1.6 \times 10^5$ km). The horizontal axis shows the wavelength direction (blue is to the left), and the width is 24 pixels in the CCDs of EIS, which corresponds to about 0.54 Å in the wavelength range. The spectra are taken at (A) 02:24:49 UT, (B) 02:25:21 UT, (C) 02:25:52 UT, (D) 02:26:24 UT, and (E) 02:26:56 UT, respectively. The flare core site is seen as very bright horizontal bands in the spectra, and it is saturated in the He II line. BS1 is located just south of the flare core region, and it drifts in the slit direction (southward) with a velocity of about 50 km s^{-1}. The flare cores are seen as bloblike bright features in all the lines used for the raster.

Figure 3 (*bottom panels*) shows the spectra of the blueshifted regions in the He II (*left*) and Fe XV (*right*) windows. The histograms shown with the solid lines are the observed spectra integrated over the blueshifted region sandwiched between the two white horizontal lines in the top panels for each emission line. The spectra are normalized with their maximum intensities. We fitted the spectra with Gaussian functions. For each window, the spectrum is divided into a main component (*dotted line*) and a blueshifted component (*solid line*). The black thin and thick arrows point to the peaks of the main and blueshifted components, respectively. The Doppler velocity is determined by the displacement between the blueshifted and the main components. Although the main components themselves show displacements compared to the profiles of a quiet region (e.g., the bottom part of the FOVs) of less than 5 km s^{-1}, they are small compared with the blueshifted phenomena and, therefore, we do not take them into the following considerations. The He II and Fe XV lines recorded Doppler velocities of about 280 and 240 km s^{-1}, respectively. For BS1, the blueshifted components are brighter than the main components.

We compared the features with the SOT data to investigate the relation between BS1 and the flare kernels. We often observe upflow motion, associated with chromospheric evaporation (Neupert 1968; Hirayama 1974; Antiochos & Sturrock 1978; Antonucci et al. 1982; Canfield & Gunkler 1985), at the footpoints of flare loops. They result from sudden pressure enhancement due to bombardment by nonthermal particles and/or conduction from the coronal flare kernels. Milligan et al. (2006) reported that the upflows of about 110 km s^{-1} in the Fe XIX line ($\log T \approx 6.9$) were observed with the *Reuven Ramaty High-Energy Solar Spectroscopic Imager* (*RHESSI*; Lin et al. 2002) at the flare kernels.

Figure 4 (*top panels*) shows the Ca II (H-line) images. We can see a two-ribbon structure that shows an inverse S-shape in the east-west direction. The crosses in the panels point to the positions of BS1 observed with EIS. The *x*-coordinate corresponds to the slit position at that time, and the *y*-coordinate is the front position (i.e., the southern end) of BS1 seen in the Fe XV line. We cannot see any correspondences between BS1 and the bright features seen in the SOT images, such as the flare ribbons. Therefore, BS1 is not related to the evaporation flow.

We compared the EIS data with the SXR images obtained with XRT. Figure 4 (*bottom panels*) shows these images. As we mentioned, we can see a plasmoid ejection, as marked with arrows. It lies horizontally and is ejected from the flare core site in the southwest direction. The crosses in the panels again indicate the front positions of BS1 determined with the Fe XV window. We can see a remarkable correspondence in all the frames between the positions of BS1 and those of the plasmoid ejection. The ejected plasmoid travels in the XRT images with a velocity of about 90 km s^{-1}, which is roughly consistent with the drift speed of BS1. Therefore, we conclude that BS1 originates from the plasmoid ejection.

As we mentioned above, the timing of BS1 just corresponds to the first impulsive radio burst observed with NoRP, which supports the plasmoid-induced reconnection model. BS1 showed Doppler and drift velocities of about 240–280 and 50–90 km s^{-1}, respectively, which indicate that the combined velocity was about 250–300 km s^{-1}. This value is consistent with the velocities that have been previously reported (e.g., Shibata et al. [1995] examined eight X-ray plasmoid ejections observed with *Yohkoh* and found that the apparent velocity was 50–400 km s^{-1}).

3.2. *The Southern Feature—BS2*

Figure 5 (*top panels*) shows time sequences of the spectra in the Fe XV and Ca XVII windows. Solar north is up, and shorter wavelength (i.e., blueward) is to the left. The size of each spectrum is 224″ along the slit (vertical), and 24 pixels in the EIS CCDs (horizontal). The displacement between CCD-A and CCD-B was corrected. The times of the spectra are taken at (*a*) 02:22:11 UT, (*b*) 02:22:43 UT, (*c*) 02:23:14 UT, (*d*) 02:23:46 UT, and (*e*) 02:24:18 UT, respectively.

The flare core site is seen as two very bright bands in these spectra. BS2 appeared from 02:22:11 to 02:24:18 UT and went out of the EIS FOV just before the first impulsive radio burst was observed with NoRP (see Fig. 1). They started to appear at 200″ south of the disk center, which is about 100″ south of the flare core region. They travel along the slit, i.e., southward, with a velocity of about 450 km s^{-1}. Furthermore, as seen in Figure 5 (*top panels*), these blueshifted features broaden widely in the blue wings of the lines. These features were observed only in the Fe XV and Ca XVII windows, which are the two hottest lines contained in the raster. Therefore, the plasma-generating BS2 must be heated more than about 2 MK.

Figure 5 (*middle panels*) shows the spectra of the blueshifted regions in the Fe XV and Ca XVII windows. The histograms shown

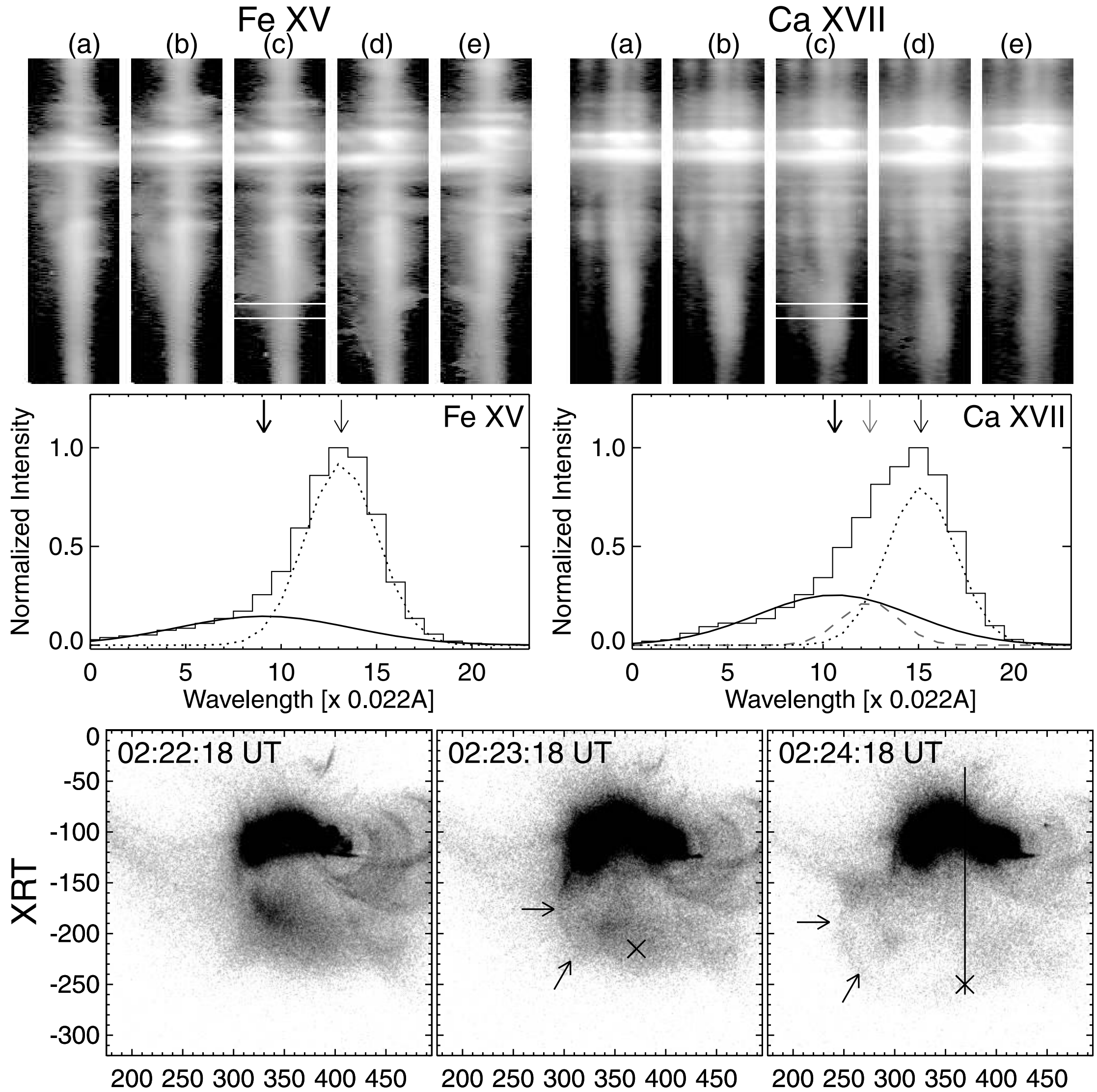

FIG. 5.—Southern blueshift (BS2). *Top*: Time-sequenced spectra of Fe XV (*left*) and Ca XVII (*right*) windows observed with *Hinode* EIS. The time of each panel is (*a*) 02:22:11 UT, (*b*) 02:22:43 UT, (*c*) 02:23:14 UT, (*d*) 02:23:46 UT, and (*e*) 02:24:18 UT. Solar north is up, and blue is to the left. The size of each window is 224″ along the EIS slit (vertical) and 24 pixels in the CCDs of EIS, which corresponds to 0.54 Å in the wavelength scale (horizontal). The displacement between CCD-A and CCD-B was corrected. *Middle*: Normalized spectra at BS2 in Fe XV (*left*) and Ca XVII (*right*) windows. The solid histograms show the spectra averaged over the region sandwiched between the two horizontal white lines in the top panels. The dotted and solid black lines are the fitting results that represent the main and the blueshift components of the line. The peaks of each line are shown with thin and thick arrows. The gray dashed line in the right panel shows the Fe XI component, and the peaks are indicated by thin gray arrows. *Bottom*: Soft X-ray negative images taken with the *Hinode* XRT. The arrows show the front of the wavelike ejection. Crosses (×) represent BS2 determined by the Fe XV line. The vertical line in the bottom right panel shows the position of the EIS slit.

with solid lines are the observed spectra integrated over the region sandwiched between the two white lines in the top panels for each line. The spectra are normalized with the maximum intensities. We fitted the spectra and divided them into several components. We assumed that all the components follow Gaussian functions.

For the Fe XV window, the spectrum is divided into Fe XV main component (*dotted line*) and the blueshifted component (*solid line*). The black thin and thick arrows point to the peaks of the main and blueshifted components, respectively. The Ca XVII window (*middle right panel*) contains Fe XI and O V lines as well as the target Ca XVII line. We can see Fe XI and O V lines discretely in the quiet region, while we can see the blended emission with the Ca XVII lines in the BS2 region. Therefore, we have to remove those components before we discuss the blueshift component of the Ca XVII line. First, we do not take the O V component into consideration, since we cannot see the component at all for the blueshifted region. The line is sensitive to the low-temperature plasma ($\log T$ is 5.4), and the absence is consistent with the fact that BS2 is hot. Second, we estimate the Fe XI component in the Ca XVII window. Since the Fe XI emission line in the Ca XVII window (192.8 Å) and the left peak (i.e., the peak with the shorter wavelength) of the Fe XI doublet (188.2 Å) are a density insensitive line pair, we can estimate the intensity and the line shift compared to the quiet region from the profile of the Fe XI lines in the Fe XI window. In Figure 5 (*middle right panel*) we show them with the gray dashed line. The Fe XI component also do not show blueshift at all. The gray arrows point to the peak positions of the Fe XI in the Ca XVII window. Then, after the subtraction of the Fe XI component, we divided the spectrum into the Ca XVII main component (*dotted line*) and the blueshifted component (*solid line*). The black thin and thick arrows again point to the peaks of the Ca XVII main and the blueshifted components, respectively.

The peaks of the BS2 components shifted 0.089 Å for the Fe xv line and 0.099 Å for the Ca xvii line, which correspond to Doppler velocities of about 90 and 150 km s^{-1}, respectively. The blueshifted components of both lines broaden widely and have wide FWHM of about 0.24 Å for the Fe xv line and about 0.21 Å for the Ca xvii line. The very wide FWHM of the blueshifted components indicates that BS2 has a large velocity field along the line of sight. These features in the spectra are very different from those of BS1.

We compared BS2 with the coronal features seen in the XRT images. We expect plasma motion in the XRT images at the same position as BS2, since XRT is sensitive to high-temperature plasma observed with the EIS Fe xv and Ca xvii spectra. Figure 5 (*bottom panels*) shows the XRT thin-Be filter images of the flare. The arrows point to the front of the XRT arc-shaped ejection, which is traveling in the southeast direction with a velocity of about 650 km s^{-1}. This ejection was faint compared with the other ejections seen in the XRT and *TRACE* images. The shape and the traveling direction are also different from the others that showed the rod-shaped structure and traveled in the southwest direction, similar to that associated with BS1. These features of the ejection resemble the X-ray waves discovered with *Yohkoh* SXT, and this disturbance is possibly generated by the MHD fast-mode shock. We roughly estimated the Alfvénic Mach number of BS2, using the same method as Narukage et al. (2002), and found it to be about 1.4. This result indicates that the XRT wavelike phenomena and BS2 might be a weak MHD fast-mode shock. The detailed analysis and theoretical treatment of the shock are beyond the scope of this paper. The observational confirmation of the density and temperature jumps caused by the passage of the shock waves will be discussed in a future paper.

The crosses in the panels show the position of BS2. The horizontal positions (*x*-coordinate) correspond to the EIS slit position. We can clearly see the correspondence between BS2 and the ejection as part of a coronal shock wave and, therefore, we conclude that BS2 is associated with the wavelike phenomenon. Furthermore, a halo-type coronal mass ejection (CME) associated with the flare was observed with the Large Angle Spectrometric Coronagraph Experiment (LASCO) on board *SOHO* (see the *SOHO* LASCO CME online catalog;[7] Yashiro et al. 2004). The EIT wave travels in almost all directions from the flare site, and the clearest disturbance is seen traveling with a speed of about 570 ± 150 km s^{-1} in the southeast direction, which is almost the same as that of the XRT wave. Figure 6 shows the running differences of the EIT images. The 02:24:33 UT image (*bottom left panel*) suffered from scattered light in the telescope and, therefore, the wave front is unclear. In the XRT image (*top left panel*) the front of the XRT wave is indicated by the solid line, and the wave is estimated to reach the dashed line position at 02:36 UT. In the 02:36:01 UT image (*bottom right panel*) the expected position of the XRT wave is also shown by the dashed line, and we can see that the front of the EIT wave is located slightly inside of the XRT wave position (*dashed line*).

BS2 recorded a Doppler velocity of about 100 km s^{-1} while the drift velocity along the slit is about 450 km s^{-1}. This implies that BS2 was traveling with a velocity of about 460 km s^{-1} and with an elevation angle of 13° from the plane of the sky, although the Doppler velocity (100 km s^{-1}) was derived from only two points of measurement. The velocity of 460 km s^{-1} is slower than the typical velocity of Moreton waves and/or X-ray waves. This

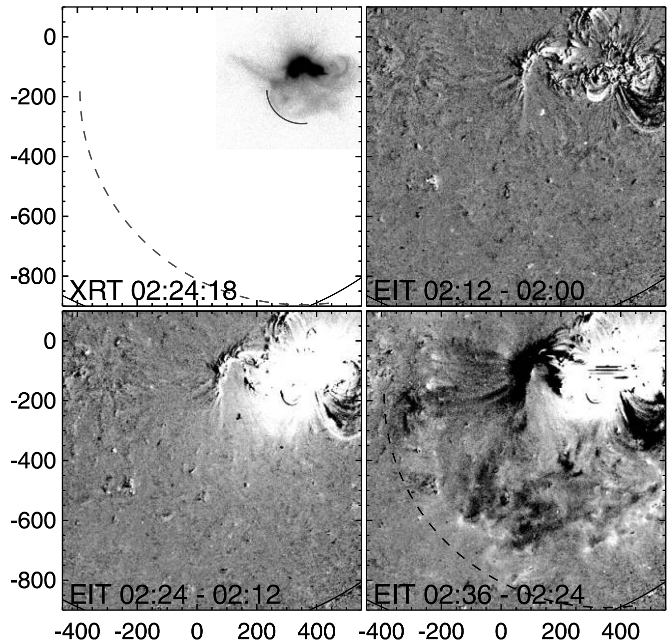

Fig. 6.—XRT image (*top left panel*) and running differences of EIT images (*other panels*). The top right panel shows the image at 02:12 UT with that of 02:00 UT subtracted. Differencing is continued in the remaining panels. The white oval region in the bottom left panel is mainly due to scattered light in the telescope. In the top left panel the XRT arc-shaped ejection is indicated by the solid line, and it is estimated to reach the dashed line at 02:36 UT. The estimated position is indicated in the bottom right panel.

is because the slit direction (north-south) is different from the direction of the arc-shaped ejection.

4. SUMMARY AND CONCLUSIONS

We found two kinds of strongly blueshifted features that were observed with *Hinode* EIS to be associated with the 2006 December 13 flare. BS1 was bright in all observed lines used for the raster, and drifted southward, that is, along the slit, at a velocity of about 50 km s^{-1}. The Doppler velocity is about 250 km s^{-1}. They are associated with the plasmoid ejection seen in XRT, while there are no corresponding flare ribbons in the Ca ii (H-line) images obtained with SOT. Therefore, we concluded that BS1 is the ejected plasma and is not an evaporation flow. Moreover, BS1 appears at the time of the first radio burst, which supports the plasmoid-induced reconnection model that shows the correlation between acceleration of plasmoids/filaments and bursts of nonthermal emissions.

BS2, on the other hand, was very faint, and showed spectra that broaden in the wavelength space. The center of the blueshifted component recorded a Doppler velocity of about 100 km s^{-1}; the drift velocity along the slit is about 450 km s^{-1}. These components are observed only in the hottest lines of the raster observation (Fe xv and Ca xvii) and, therefore, the plasmas must be heated to more than 2 MK. The BS2 region corresponds to the propagation of the coronal wavelike ejection seen in XRT images. The ejection is thought to be a MHD fast-mode shock wave, and it is the first successful spectroscopic observation of such a shock wave associated with a flare.

We first acknowledge an anonymous referee for her/his useful comments and suggestions. *Hinode* is a Japanese mission

[7] See http://cdaw.gsfc.nasa.gov/CME_list.

developed and launched by ISAS/JAXA, collaborating with NAOJ as domestic partner and NASA and STFC (UK) as international partners. Scientific operation of the *Hinode* mission is conducted by the *Hinode* science team organized at ISAS/JAXA. This team mainly consists of scientists from institutes in the partner countries. Support for the postlaunch operation is provided by JAXA and NAOJ (Japan), STFC (UK), NASA, ESA, and NSC (Norway). This work was partly carried out at the NAOJ Hinode Science Center, which is supported by the Grant-in-Aid for Creative Scientific Research "The Basic Study of Space Weather Prediction" from MEXT, Japan (17GS0208, Head Investigator: K. Shibata), generous donations from Sun Microsystems, and NAOJ internal funding. J. L. C. acknowledges the award of a Leverhulme Emeritus Fellowship.

REFERENCES

Antiochos, S. K., & Sturrock, P. A. 1978, ApJ, 220, 1137
Antonucci, E., et al. 1982, Sol. Phys., 78, 107
Aschwanden, M. J. 2002, Space Sci. Rev., 101, 1
Canfield, R. C., & Gunkler, T. A. 1985, ApJ, 288, 353
Carmichael, H. 1964, in Proc. AAS-NASA Symp., ed. W. N. Hess (NASA SP-50; Washington: NASA), 451
Culhane, J. L., et al. 2007, Sol. Phys., 243, 19
Delaboudinière, J.-P., et al. 1995, Sol. Phys., 162, 291
Domingo, V., Fleck, B., & Poland, A. I. 1995, Sol. Phys., 162, 1
Eto, S., et al. 2002, PASJ, 54, 481
Golub, L., et al. 2007, Sol. Phys., 243, 63
Handy, B. N., et al. 1999, Sol. Phys., 187, 229
Hirayama, T. 1974, Sol. Phys., 34, 323
Hudson, H. S., Khan, J. I., Lemen, J. R., Nitta, N. V., & Uchida, Y. 2003, Sol. Phys., 212, 121
Imada, S., et al. 2007, PASJ, 59, S793
Isobe, H., et al. 2007, PASJ, 59, S807
Kahler, S. W., Moore, R. L., Kane, S. R., & Zirin, H. 1988, ApJ, 328, 824
Khan, J. I., & Aurass, H. 2002, A&A, 383, 1018
Khan, J. I., & Hudson, H. S. 2000, Geophys. Res. Lett., 27, 1083
Kopp, R. A., & Pneuman, G. W. 1976, Sol. Phys., 50, 85
Korendyke, C. M., et al. 2006, Appl. Opt., 45, 8674
Kosugi, T., et al. 2007, Sol. Phys., 243, 3
Kubo, M., et al. 2007, PASJ, 59, S779
Lang, J., et al. 2006, Appl. Opt., 45, 8689
Lin, R. P., et al. 2002, Sol. Phys., 210, 3
Milligan, R. O., Gallagher, P. T., Mathiudakis, M., & Keenan, F. P. 2006, ApJ, 642, L169
Moreton, G. E. 1960, AJ, 65, 494
Morimoto, T., & Kurokawa, H. 2003, PASJ, 55, 1141
Nakajima, H., et al. 1985, PASJ, 37, 163
Narukage, N., et al. 2002, ApJ, 572, L109
Neupert, W. M. 1968, ApJ, 153, L59
Ogawara, Y., et al. 1991, Sol. Phys., 136, 1
Ohyama, M., & Shibata, K. 1998, ApJ, 499, 934
Schrijver, C. J., et al. 1999, Sol. Phys., 187, 261
Shibasaki, K., Ishiguro, M., & Enome, S. 1979, Proc. Res. Inst. Atmos., 26, 117
Shibata, K. 1999, Ap&SS, 264, 129
Shibata, K., Masuda, S., Shimojo, M., Hara, H., Yokoyama, T., Tsuneta, S., Kosugi, T., & Ogawara, Y. 1995, ApJ, 451, L83
Shibata, K., & Tanuma, S. 2001, Earth Planets Space, 53, 473
Smith, S. F., & Harvey, K. L. 1971, in Physics of the Solar Corona, ed. C. J. Macris (Dordrecht: Reidel), 156
Sterling, A. C., & Moore, R. L. 2004, ApJ, 613, 1221
———. 2005, ApJ, 630, 1148
Sturrock, P. A. 1966, Nature, 211, 695
Su, Y., et al. 2007, PASJ, 59, S785
Thompson, B. J., et al. 2000, Sol. Phys., 193, 161
Torii, C., Tsukiji, Y., Kobayashi, S., Yoshimi, N., Tanaka, H., & Enome, S. 1979, Proc. Res. Inst. Atmos., 26, 129
Tsuneta, S. 1997, ApJ, 483, 507
Tsuneta, S., et al. 1991, Sol. Phys., 136, 37
———. 2007, Sol. Phys., 249, 167
Uchida, Y. 1968, Sol. Phys., 4, 30
———. 1970, PASJ, 22, 341
Uchida, Y., Altschuler, M. D., Newkirk, G., Jr. 1973, Sol. Phys., 28, 495
Warmuth, A., Mann, G., & Aurass, H. 2005, ApJ, 626, L121
Warmuth, A., Vršnak, B., Magdalenić, J., Hanslmeier, A., & Otruba, W. 2004a, A&A, 418, 1101
———. 2004b, A&A, 418, 1117
Yashiro, S., Gopalswamy, N., Michalek, G., St. Cyr, O. C., Plunkett, S. P., Rich, N. B., & Howard, R. A. 2004, J. Geophys. Res., 109, A07105